Protein tyrosine phosphatase non-receptor type 2 controls colorectal cancer development

Katkeviciute, Egle ; Hering, Larissa ; Montalban-Arques, Ana ; Busenhart, Philipp ; Schwarzfischer, Marlene ; Manzini, Roberto ; Conde, Javier ; Atrott, Kirstin ; Lang, Silvia ; Rogler, Gerhard ; Naschberger, Elisabeth ; Schellerer, Vera S ; Stürzl, Michael ; Rickenbacher, Andreas ; Turina, Matthias ; Weber, Achim ; Leibl, Sebastian ; Leventhal, Gabriel E ; Levesque, Mitchell Paul ; Boyman, Onur ; Scharl, Michael ; Spalinger, Marianne R

Abstract: Protein tyrosine phosphatase non-receptor type 2 (PTPN2) recently emerged as a promising cancer immunotherapy target. We set to investigate the functional role of PTPN2 in the pathogenesis of human colorectal carcinoma (CRC) as its role in immune-silent solid tumors is poorly understood. We demonstrate that in human CRC, increased PTPN2 expression and activity correlated with disease progression and decreased immune responses in tumor tissues. Particularly, stage II and III tumors displayed enhanced PTPN2 protein expression in tumor-infiltrating T-cells and increased PTPN2 levels negatively correlated with PD1, CTLA4, STAT1 and granzyme A. In vivo, T-cell and dendritic cell-specific PTPN2 deletion reduced tumor burden in several CRC models by promoting CD44+ effector/memory T-cells, as well as CD8+ T-cell infiltration and cytotoxicity into the tumor. In direct relevance to CRC treatment, T-cell-specific PTPN2 deletion potentiated anti-PD-1 efficacy and induced anti-tumor memory formation upon tumor re-challenge in vivo. Our data suggest a role for PTPN2 in suppressing anti-tumor immunity and promoting tumor development in CRC patients. Our in vivo results uncover PTPN2 as a key player in controlling immunogenicity of CRC, with the strong potential to be exploited to promote cancer immunotherapy.

DOI: https://doi.org/10.1172/JCI140281

Protein tyrosine phosphatase non-receptor type 2 controls colorectal cancer development

Egle Katkeviciute[1], Larissa Hering[1], Ana Montalban-Arques[1], Philipp Busenhart[1], Marlene Schwarzfischer[1], Roberto Manzini[1], Javier Conde[1], Kirstin Atrott[1], Silvia Lang[1], Gerhard Rogler[1,2] Elisabeth Naschberger[3], Vera S. Schellerer[4], Michael Stürzl[3], Andreas Rickenbacher[5], Matthias Turina[5], Achim Weber[6], Sebastian Leibl[6], Gabriel E Leventhal[7], Mitchell Levesque[8], Onur Boyman[9,10], Michael Scharl[1,2*] and Marianne R Spalinger[1]

The authors have declared that no conflict of interest exists

[1] Department of Gastroenterology and Hepatology, University Hospital Zurich, University of Zurich, Zurich, Switzerland
[2] Zurich Center for Integrative Human Physiology, University of Zurich, Zurich, Switzerland
[3] Division of Molecular and Experimental Surgery, University Medical Center of Erlangen, Friedrich-Alexander-University Erlangen-Nürnberg, Erlangen, Germany
[4] Department of Surgery, University Medical Center of Erlangen, Friedrich-Alexander-University Erlangen-Nürnberg, Erlangen, Germany
[5] Department of Visceral and Transplant Surgery, University Hospital Zurich, Zurich, Switzerland
[6] Department of Pathology, University Hospital Zurich, Zurich, Switzerland
[7] Department of Civil and Environmental Engineering, Massachusetts Institute of Technology (MIT), Cambridge, USA
[8] Department of Dermatology, University Hospital Zurich, Zurich, Switzerland
[9] Department of Immunology, University Hospital Zurich, Zurich, Switzerland
[10] Faculty of Medicine, University of Zurich, Zurich, Switzerland

***Correspondence**: Prof Dr. Michael Scharl, Department of Gastroenterology and Hepatology, University Hospital Zurich, Rämistrasse 100, 8091 Zurich, Switzerland. Michael.Scharl@usz.ch. +41-44-255-3419

Abstract

Protein tyrosine phosphatase non-receptor type 2 (PTPN2) recently emerged as a promising cancer immunotherapy target. We set to investigate the functional role of PTPN2 in the pathogenesis of human colorectal carcinoma (CRC) as its role in immune-silent solid tumors is poorly understood. We demonstrate that in human CRC, increased PTPN2 expression and activity correlated with disease progression and decreased immune responses in tumor tissues. Particularly, stage II and III tumors displayed enhanced PTPN2 protein expression in tumor-infiltrating T-cells and increased PTPN2 levels negatively correlated with PD-1, CTLA4, STAT1 and granzyme A. In vivo, T-cell and dendritic cell-specific PTPN2 deletion reduced tumor burden in several CRC models by promoting $CD44^{+}$ effector/memory T-cells, as well as CD8+ T-cell infiltration and cytotoxicity into the tumor. In direct relevance to CRC treatment, T-cell-specific PTPN2 deletion potentiated anti-PD-1 efficacy and induced anti-tumor memory formation upon tumor re-challenge in vivo. Our data suggest a role for PTPN2 in suppressing anti-tumor immunity and promoting tumor development in CRC patients. Our in vivo results uncover PTPN2 as a key player in controlling immunogenicity of CRC, with the strong potential to be exploited to promote cancer immunotherapy.

Keywords: Colorectal cancer; TCPTP; PTPN2; T cells; immunotherapy.

Introduction

Colorectal carcinoma (CRC) is the third most frequent malignancy and the second leading cause of cancer-related deaths worldwide (1, 2). In 2018, more than 1.8 million patients were newly diagnosed with CRC and despite improved 5-year survival, the estimated number of CRC-related deaths accumulated to 881,000 (3-6). Successful immunotherapeutic interventions in other solid cancers, such as melanoma and lung carcinoma have exploited their tumor microenvironment, which contains high numbers of immune cells, such as T-cells, natural killer (NK) cells and antigen-presenting cells (7, 8). The majority of CRC, however, lack prominent immune infiltrates and only about 4% of all CRC cases respond to immunotherapies (2, 9). Immunogenic CRC are characterized by mismatch-repair-deficiency and high microsatellite instability resulting in a high tumor mutation rate (2). In contrast, the majority of CRC tumors exhibit low immunogenicity and evade eradication by circulating T-cells and NK cells via expression of immunosuppressive modulators such as TGFβ, recruitment of Tregs and promotion of myeloid-derived suppressor cells (10). This absence of anti-tumor immune cell recruitment is the main hurdle for successful immunotherapy, which generates a high need for effective immune modulators to render colorectal tumors more immunogenic (2).

Protein tyrosine phosphatase non-receptor type 2 (PTPN2) has recently been suggested as a possible target for tumor therapy (11-13). PTPN2 is a ubiquitously expressed anti-inflammatory protein known to regulate pro-inflammatory signaling pathways by direct dephosphorylation, including several Janus kinases, signal transducer and activator of transcription (STAT) family members and others (14-17). Total body deficiency of PTPN2 in mice causes severe systemic inflammation and

death within 3-5 weeks after birth, thus, mice with cell type-specific PTPN2 deletions have been developed (18).

We have recently shown that loss of PTPN2 in myeloid cells and intestinal epithelial cells reduce tumor load and promote immune responses against tumors in a model of colitis-associated colon cancer by increasing IL-1β production and elevating immunogenicity of the tumor (19). Tumor cell-specific and T-cell-specific PTPN2 deletion has been reported to reduce tumor load in subcutaneous tumor models using melanoma and CRC cell lines as well as in mammary tumor models (11-13). In humans, reduced PTPN2 expression correlated with better treatment response in T-cell acute lymphoblastic leukemia in children (20). However, the molecular role of PTPN2 in T-cells in the context of hard-to-treat solid tumors has not been studied in depth and little is known about its role in human CRC.

Here, we demonstrate that increased PTPN2 expression in human CRC tissue, and especially in infiltrating lymphocytes, correlates with reduced levels of T-cell activity and cytotoxicity. Further, we show that PTPN2 deletion in T-cells lowers tumor load in orthotopic and heterotopic CRC and melanoma mouse models and enhances T-cell activity, infiltration and cytotoxicity, thus rendering tumors more immunogenic. Finally, PTPN2 deletion in T-cells potentiates the efficacy of anti-PD-1 treatment, resulting in more effective tumor clearance and immune memory formation. These data suggest PTPN2 as a very promising stand-alone or combination therapy target in CRC.

Results

PTPN2 expression is increased in CRC patients

To investigate the importance of PTPN2 in the pathogenesis of human CRC, we first analyzed PTPN2 protein levels in colonic non-tumor versus tumor tissues from CRC patients using immunohistochemistry (IHC). While PTPN2 expression in non-tumor tissues was moderate, we observed significantly enhanced levels of PTPN2 in CRC tumor tissues of all stages (Figure 1A). PTPN2 phosphatase activity was increased in CRC tumor tissues compared to non-tumor tissues from the same patient (Figure 1B). Consistent with enhanced PTPN2 activity, levels of pSTAT1, a direct PTPN2 target, were low and inversely correlated with PTPN2 protein expression (Figure 1C).

PTPN2 was mainly expressed in tumor cells, but interestingly in stages I-III we observed increasing numbers of CD3+ cells, which were positive for PTPN2, while PTPN2 expression in the cancer cells was not changed across the tumor stages. Stage IV tissue however showed lower numbers of PTPN2+ infiltrating CD3+ cells (Figure 1D), likely due to the overall reduced levels of CD3+ cells. Since PTPN2 and pSTAT1 are suggested to modulate T-cell recruitment and activity (11, 21), we investigated whether *PTPN2* expression correlates with T-cell associated genes, such as *STAT1, CXCL11* and *granzyme A,* which are required for T-cell activity, recruitment and cytotoxicity, respectively. We observed an inverse correlation in stages I-III for ratios of *STAT1/PTPN2*, *CXCL11/PTPN2* and *GZMA/PTPN2* (Figure 1E). Stage IV tumors, however, showed a direct correlation for all three genes (Figure 1E), indicating a change in immune activity in metastatic tumors and highlighting the observation of fewer PTPN2+ infiltrating immune cells in this stage. Stage IV tumors emerge upon significant changes in the expression of various genes that not only enables tumor cell

migration and metastasis formation, but also to evade detection by the immune system. These changes not only affect gene expression in tumor cells, but likely also affect the activity and function of PTPN2 not only in tumor but also in surrounding immune cells, specifically T cells. Thus, it is not surprising that the expression of the analyzed factors, *STAT1*, *CXCL11*, and *GZMA,* which are associated with immune cell infiltration and activation, show an opposite correlation with PTPN2 in stage IV tumors.

Finally, we explored PTPN2 protein expression and localization of checkpoint molecules in primary CRC, liver metastasis and melanoma. For primary CRC, we observed that high PTPN2 expression in CRC tumor tissues correlated with low checkpoint molecules expression, similar to liver metastasis, where low PTPN2 expression within tumor tissues was associated with strong PD-1 and CTLA4 staining (Figures 1F and S1A-B). On the contrary, we observed high PTPN2 expression, which slightly positively correlated with expression of PD-1 in melanoma, showing that highly immunogenic tumors show different PD-1 association with PTPN2 (Figure S1A). Taken together, these patient studies demonstrate increased PTPN2 levels in immune cells in progressing CRC tumors, unveiling that PTPN2 could be a mediator of decreased immunogenicity of CRC.

Loss of PTPN2 in T-cells reduces tumor burden in the AOM/DSS tumor model

Our results from patients suggest a crucial role of PTPN2 in immune cells during CRC development. To confirm this hypothesis, we investigated the role of PTPN2 in T-cells in CRC mouse models. In a first approach, we applied the AOM/DSS CRC model in *Ptpn2*$^{fl/fl}$*Cd4*$^{Cre+/-}$ (referred to as ΔT in figures) mice lacking PTPN2 specifically in both

CD4+ and CD8+ T cells (22, 23). *Ptpn2*$^{fl/fl}$ (WT) littermates not carrying the Cre construct were used as controls (Figure 2A).

In AOM/DSS-treated WT mice, we observed prominent tumor growth in the distal part of the colon when compared to *Ptpn2*$^{fl/fl}$*Cd4*$^{Cre+/-}$ littermate controls, while the controls did not show any visual differences between genotypes (Figures 2B). The size and number of tumors were significantly reduced in *Ptpn2*$^{fl/fl}$*Cd4*$^{Cre+/-}$ mice compared to their WT littermate controls (Figure 2C). H&E staining of colon sections showed highly increased immune cell infiltration into tumor tissues in *Ptpn2*$^{fl/fl}$*Cd4*$^{Cre+/-}$ mice compared to WT littermates (Figure 2D) and IHC staining of CD3 demonstrated augmented accumulation of T-cells into the tumors of these mice (Figure 2E).

RNA sequencing of colon tissues from water (normal tissue) and AOM/DSS-treated (non-tumor and tumor tissue) WT and *Ptpn2*$^{fl/fl}$*Cd4*$^{Cre+/-}$ mice revealed that AOM/DSS treatment in *Ptpn2*$^{fl/fl}$*Cd4*$^{Cre+/-}$ mice showed the highest change in expression of genes involved in CD8^{+} T-cell signaling, cytotoxicity, and infiltration, including STAT1, IFNγ, the family of granzymes, checkpoint molecules, and chemokines (Figure 2F and Supplementary Figure 2A). We confirmed the significant changes in chemokines expression observed in the RNA sequencing using quantitative (q)PCR (Supplementary Figure 2B). Similarly to the data obtained in RNA sequencing, CXCL9, CXL11, CXCR3 and CXCR5 chemokines were significantly upregulated in the tumor tissue from *Ptpn2*$^{fl/fl}$*Cd4*$^{Cre+/-}$ mice comparing to their littermate controls. Collectively, these findings indicate that PTPN2 deletion in T-cells leads to changes in the cytotoxic T-cell compartment in the inflammation-dependent AOM/DSS CRC model.

PTPN2 regulates expression, activation and tumor infiltration of CD8$^+$ cytotoxic T-cells

To further investigate the alterations caused by PTPN2 deletion on T-cell function/activation, we examined CD4$^+$ and CD8$^+$ T-cells in detail. IHC and flow cytometry analysis of CD4$^+$ T-cells in healthy colon, inflamed non-tumor, and tumor tissues did not reveal significant differences in the frequencies of CD4$^+$ T-cells between *Ptpn2$^{fl/fl}$Cd4$^{Cre+/-}$* and WT mice (Figure 3A). Nevertheless, effector/memory CD4$^+$ T-cells were increased in spleen and mLN of *Ptpn2$^{fl/fl}$Cd4$^{Cre+/-}$* mice independent of the treatment (Figure 3B). Yet no signs of microscopic inflammation or morphologic changes were detectable in the colon of unchallenged *Ptpn2$^{fl/fl}$Cd4$^{Cre+/-}$* mice. Flow cytometry showed a clear increase of Th1 (CD4$^+$IFNγ^+) cells, while Th2 (CD4$^+$IL-4$^+$), Th17 (CD4$^+$IL-17$^+$) and Treg (CD4$^+$FoxP3$^+$) cells did not show significant changes between *Ptpn2$^{fl/fl}$Cd4$^{Cre+/-}$* mice and WT littermate controls (Figure 3C and Figure S3A).

Of note, we found increased infiltration and frequency of CD8$^+$ T-cells in inflamed non-tumor and tumor tissues in *Ptpn2$^{fl/fl}$Cd4$^{Cre+/-}$* mice by IHC and flow cytometry (Figures 3D). This increase in CD8+ T cell infiltration is well in line with the upregulation of chemokines/chemokine receptors observed in the tumor tissue. A predominant fraction of CD8$^+$ T-cells were activated effector/memory (CD8$^+$CD44$^+$CD62L$^-$) T-cells in both, water control and AOM/DSS-treated mice in the spleen and mLNs (Figure 3E). Although comparable frequencies of PTPN2-deficient CD8$^+$ T-cells were activated in water and AOM/DSS mice, the frequency of granzyme B-positive cells was clearly increased specifically in tumor tissue, an effect completely absent in *Ptpn2$^{fl/fl}$* mice (Figure 3F and Figure S3A-C). Similar to CD4$^+$ T-cells, PTPN2-deficient CD8$^+$ T-cells

expressed more IFNγ compared to those from WT, but frequencies did not differ between healthy and inflamed (non-tumor)/tumor tissues (Figure 3F).

In WT mice, the frequency of $CD4^+PD\text{-}1^+$ T-cells but not $CD8^+PD\text{-}1^+$ T-cells, was significantly increased in non-tumor and tumor tissue when compared to healthy tissue. In contrast, the frequency of $CD4^+PD\text{-}1^+$ cells did not differ between tissues from water and AOM/DSS-treated *Ptpn2*$^{fl/fl}$*Cd4*$^{Cre+/-}$ mice and was overall significantly lower than in WT littermates (Figure 3F). Nevertheless, there was a clear increase of PD-1 on *Ptpn2*$^{fl/fl}$*Cd4*$^{Cre+/-}$ $CD8^+$ T-cells in inflamed non-tumor colon and tumor tissues compared to healthy colon tissues, but was still lower than in WT mice (Figure 3F).

PTPN2 T-cell deficiency reduces tumor burden independent from inflammation

We next assessed tumor burden in inflammation-independent models of CRC, namely the orthotopic MC38 cecum injection model and the genetic APCmin mouse model.

Remarkably, using the cecum injection model, about 60% of *Ptpn2*$^{fl/fl}$*Cd4*$^{Cre+/-}$ mice completely cleared the tumors and the remaining tumors were relatively small, whereas WT mice failed to control the tumors (Figures 4A-B). IHC and flow cytometry analysis of $CD8^+$ T-cells showed enhanced infiltration of $CD8^+$ T-cells into tumors in *Ptpn2*$^{fl/fl}$*Cd4*$^{Cre+/-}$ mice compared to WT littermate controls (Figures 4C). Again, we observed increased chemokines expression in tumors from *Ptpn2*$^{fl/fl}$*Cd4*$^{Cre+/-}$ mice, which further supports increased $CD8^+$ T-cells infiltration into tumor, as mechanism for reduced tumor burden (Supplementary Figure 4A).

We observed a comparable increase in systemic $CD8^+$ T-cell activation upon loss of PTPN2 in the AOM/DSS and the cecum injection tumor models, suggesting that initial inflammation was not required for T cell activation and tumor clearance. (Figure 4D).

Furthermore, we found similar expression of cytotoxicity markers in both tumor models, including increased granzyme B and IFNγ levels in tumor tissues of *Ptpn2*$^{fl/fl}$*Cd4*$^{Cre+/-}$ compared to WT littermate controls (Figure 4E). Notably, in the cecum injection model, PD-1 expression on CD8$^+$ T-cells was significantly increased in *Ptpn2*$^{fl/fl}$*Cd4*$^{Cre+/-}$ mice compared to WT controls (Figure 4E).

In the genetic APCmin model of CRC, *Ptpn2*$^{fl/fl}$*Cd4*$^{Cre+/-}$*APCmin* mice revealed an extensive reduction of tumor burden in small intestine when compared to *Ptpn2*$^{fl/fl}$*APCmin* littermates (Figure 4F) and *Ptpn2*$^{fl/fl}$*Cd4*$^{Cre+/-}$*APCmin* exhibited healthy spleens, while spleens from *Ptpn2*$^{fl/fl}$*APCmin* mice had significantly increased spleen weight (Figure 4F) and unhealthy pale color.

Finally, to validate whether PTPN2 deletion in T-cells exerts not only local effects in the colon, but is also relevant for systemic tumors, we next applied the subcutaneous injection model using MC38 CRC and B16 melanoma cells. Consistent with our findings with *in situ* tumors, we observed slower tumor growth and reduced size and weight in *Ptpn2*$^{fl/fl}$*Cd4*$^{Cre+/-}$ mice compared to WT mice regardless of the cancer cell type, i.e. MC38 or B16 (Figure 5A-B and Figure S5A).

PTPN2-deficient CD8$^+$ T-cells are the key mediators of antitumor efficacy

Given the prominent changes in CD8$^+$ T-cells in all our data, CD8$^+$ T-cell depletion in the MC38 subcutaneous injection model abrogated the protective effect of PTPN2 deficiency resulting in similar tumor growth and terminal weight in *Ptpn2*$^{fl/fl}$*Cd4*$^{Cre+/-}$ and WT littermates (Figures 5C-D).

IHC staining and flow cytometry analysis revealed highly increased infiltration of PTPN2-deficient CD8$^+$ T-cells into the tumor in isotype-treated control mice, while

CD8$^+$ T-cells were successfully depleted in both mouse lines. (Figure 5E). Of note, we observed an inverse correlation between tumor weight and CD8$^+$ T-cell frequency in the tumor tissues in *Ptpn2*$^{fl/fl}$*Cd4*$^{Cre+/-}$ mice, while in WT mice such a correlation was not detectable. (Figure 5F).

In contrast to the drastic effects of CD8 depletion, depletion of CD4$^+$ T cells did not affect the tumor suppression capacity in *Ptpn2*$^{fl/fl}$*Cd4*$^{Cre+/-}$ mice. While in WT mice tumor growth was slightly suppressed upon CD4$^+$ T cell depletion (Figure 5G and 5H and Supplementary Figure 5A), which might result from the depletion of Tregs, however was not further investigated in this study. Flow cytometry analysis revealed complete CD4$^+$ T cells depletion in spleen and around 80% reduction in tumor tissue (Supplementary Figure 5B). The expression of Granzyme B and IFNγ was significantly higher in *Ptpn2*$^{fl/fl}$*Cd4*$^{Cre+/-}$ mice when compared to WT mice with or without CD4 depletion (Supplementary Figure 5C). Thus, CD4$^+$ T cells were not required for tumor suppression in *Ptpn2*$^{fl/fl}$*Cd4*$^{Cre+/-}$ mice.

To further investigate the anti-tumor potential of PTPN2-deficient CD8$^+$ T-cells, we injected MC38 cells into *Rag2*-deficient mice, followed by adoptive transfer of either WT or PTPN2-deficient CD8$^+$ T-cells on day 6 (Figure 6A). Remarkably, tumor growth was significantly slower in mice that received CD8$^+$ T-cells from *Ptpn2*$^{fl/fl}$*Cd4*$^{Cre+/-}$ mice, further demonstrating the prominent role of CD8$^+$ T-cells in reducing tumor load in *Ptpn2*$^{fl/fl}$*Cd4*$^{Cre+/-}$ mice (Figures 6B).

The increased anti-tumor capacity of PTPN2-deficient T cells was confirmed in an in vitro killing assay where we incubated MC38 and MC38-OVA expressing cells with *Ptpn2*$^{fl/fl}$*OT-I* or *Ptpn2*$^{fl/fl}$*Cd4*$^{Cre+/-}$*OT-I* cells. PTPN2-deficient OT-I cells were more

efficient in antigen-specific tumor killing when compared to PTPN2-proficient OT-I cells (Figure 6C).

PTPN2 deletion in dendritic cells leads to reduced tumor burden in the AOM/DSS and the orthotopic injection models

After our findings in mice lacking PTPN2 in T cells, we investigated whether deletion of PTPN2 in antigen presenting cells, specifically dendritic cells (DCs), also affects the tumor development in our colorectal cancer models. Of note our previous work showed a significant tumor reduction in mice lacking PTPN2 in myeloid cells (19), but the effect of PTPN2-depletion in dendritic cells on CRC development is still unknown.

For this aim, we first subjected *Ptpn2*$^{fl/fl}$*Cd11c*$^{Cre+/-}$ and their WT littermate controls (*Ptpn2*$^{fl/fl}$) to the AOM/DSS model where we observed a significant reduction in tumor load and enhanced CD8+ T-cell infiltration in *Ptpn2*$^{fl/fl}$*Cd11c*$^{Cre+/-}$ mice compared to their littermates (Figures 7A-C). Similar to *Ptpn2*$^{fl/fl}$*Cd4*$^{Cre+/-}$ mice, we observed enhanced levels of effector/memory T-cells in *Ptpn2*$^{fl/fl}$*Cd11c*$^{Cre+/-}$ mice (Figures 7C) suggesting that PTPN2-deficient DCs promote T-cell activation. This is well in line with a recently published study from our group (24).

Next, we applied the orthotopic MC38 cecum injection model of CRC in *Ptpn2*$^{fl/fl}$*Cd11c*$^{Cre+/-}$ and *Ptpn2*$^{fl/fl}$ mice and found similar cellular and pathologic phenotypes as observed in the AOM/DSS model, which again mirrored the situation in the *Ptpn2*$^{fl/fl}$*Cd4*$^{Cre+/-}$ tumor models. We found considerably reduced tumor load (Figure 7D), changes in the tumor morphology (Figure 7E) and significantly increased infiltration, activation and cytotoxicity of CD8^{+} T-cells. (Figures 7F-H). Thus, we

hypothesize that in *Ptpn2*$^{fl/fl}$*Cd11c*$^{Cre+/-}$ mice, activated T cells, as in *Ptpn2*$^{fl/fl}$*Cd4*$^{Cre+/-}$ mice, might mediate the reduced tumor load.

PTPN2 deletion renders tumors more susceptible to anti-PD-1 treatment

To investigate whether PTPN2 deletion makes T cells more susceptible to immunotherapy, we injected MC38 tumor cells subcutaneously into WT and *Ptpn2*$^{fl/fl}$*Cd4*$^{Cre+/-}$ mice and administered anti-PD-1 antibody at day 9, 12 and 15, when large (100-200mm^3) tumor nodules had formed (Figure 8A). Already in PTPN2-deficient mice receiving IgG isotype control, we observed reduced tumor growth, but strikingly, almost all *Ptpn2*$^{fl/fl}$*Cd4*$^{Cre+/-}$ mice treated with anti-PD-1 cleared the tumors by day 20 (Figures 8A-B). This additive effect on tumor reduction suggests that PTPN2 deletion and anti-PD-1 therapy mediates tumor reduction through distinct mechanisms. Contrarily, all WT mice reached the termination criteria due to tumor size, with or without anti-PD-1 treatment (Figure 8A-B). Additionally, tumor morphology was altered in anti-PD-1 treated *Ptpn2*$^{fl/fl}$*Cd4*$^{Cre+/-}$ mice evident by reduced cancer cell density and patches of immune cell infiltrates (Figure 8C). Anti-PD-1 treatment promoted CD8+ T cell infiltration in PTPN2-deficient mice, but not in WT (Figures 8D), indicating that PTPN2-depletion in T cells renders tumors more susceptible to checkpoint inhibitor treatment.

We further noted that the frequency of CD8$^+$PD-1$^+$ cells was significantly increased in isotype treated *Ptpn2*$^{fl/fl}$*Cd4*$^{Cre+/-}$ mice when compared to WT controls (Figure 8E). Depletion of PD-1 was successful in both WT and *Ptpn2*$^{fl/fl}$*Cd4*$^{Cre+/-}$ mice and evident in CD8$^+$ T-cells, yet the anti-PD-1 therapy had much stronger effects on tumor load in PTPN2-deficient mice. Lastly, checkpoint blockade did not change activation and

cytotoxicity of T-cells in WT mice, while *Ptpn2*$^{fl/fl}$*Cd4*$^{Cre+/-}$ mice had significantly more cytotoxic and activated T-cells upon anti-PD-1 therapy (Figures 8E).

Increased immune memory formation in *Ptpn2*$^{fl/fl}$*Cd4*$^{Cre+/-}$ mice

To investigate whether PTPN2 deletion affects tumor-specific immune cell memory, we re-challenged *Ptpn2*$^{fl/fl}$*Cd4*$^{Cre+/-}$ mice with a second injection of MC38 cells after they had cleared primary MC38 tumors after anti-PD-1 therapy. To compare primary and memory responses we also injected MC38 cells into treatment-naive *Ptpn2*$^{fl/fl}$*Cd4*$^{Cre+/-}$ mice (Figure 8F). Mice that were re-challenged with MC38 cells developed smaller tumors than the mice with primary injections, and all re-challenged mice but only few mice that received primary injections cleared the tumors (Figure 8F). Thus, PTPN2 deficiency does not only promote tumor clearance in synergy with anti-PD-1 treatment, but also induces memory responses that mediate spontaneous tumor clearance upon re-challenge.

Discussion

In this study, we demonstrate that immune cell specific PTPN2 plays an important role in the development of human CRC. Using a large collective of tissue samples from CRC patients, we show that PTPN2 protein expression and activity was highly elevated in human CRC tissue, with a marked increase in immune cells, and that high *PTPN2* gene expression correlated with reduced T-cell activity, recruitment, and cytotoxicity. Using well-defined mouse models, we verified that PTPN2 expression in T-cells and DCs dampened anti-tumor immune responses and PTPN2-deficiency led to significantly reduced tumor burden in vivo. Recent reports showed that PTPN2 silencing in T-cells led to reduced tumor load upon subcutaneous injection of MC38 and B16 cells and in mammary tumor mouse models (12, 13). While these studies showed altered T-cell differentiation and enhanced anti-tumor response upon T-cell-specific loss of PTPN2, they did not investigate human CRC tissues nor did they examine whether cells of the in situ tumor microenvironment – which are critical for determining therapy response – affect tumor growth of CRC in vivo. In contrast, our study explores the potential of PTPN2 as a therapeutic target in different CRC models that adequately represent the tumor environment and development observed in human CRC patients.

Since in the majority of CRC patients, low immunogenicity of the tumors prevents response to immunotherapies (7, 8, 25, 26), therapeutic approaches that promote the immunogenic potential provide a strong rationale for improving treatment success. Our data from primary and metastatic human CRC tissues indicate a strong correlation of local PTPN2 expression and reduced immune response. Thus, our observations in human patients suggest PTPN2 as an important target for CRC therapy.

PTPN2 is a known anti-inflammatory protein, which dephosphorylates several inflammatory mediators and prevents tissue inflammation (15-17, 21). PTPN2 deficiency in mice has previously been shown to affect pathologic immune responses as well as development of T-cells and B-cells, mediate hypersensitivity of macrophages, and enhance production of pro-inflammatory cytokines, such as IFNγ, TNF and IL-1β (18, 19, 21). We have previously described that conditional PTPN2 KO (cKO) in T cells promotes Th1 and Th17 differentiation in colitis models and resulted in increased IFNγ and IL-17 production (17). To add more, T cell cKO has been shown to promote T cell activation and promote TCR-dependent $CD8^+$T cell proliferation (14). Further, we recently demonstrated that cKO in DCs promotes Th1 differentiation and IFNγ production via upregulation of co-stimulatory molecules in PTPN2-deficient DCs (24).

Here, we demonstrate again that PTPN2 deletion in T cells and DCs increases IFNγ production, which promotes differentiation and activation of $CD4^+$ Th1 cells and increased cytotoxic ability of $CD8^+$ T-cells. Of key importance to the therapeutic potential to inhibit PTPN2 function, however, is the fact that the highly increased frequency of granzyme B-producing PTPN2-deficient $CD8^+$ T-cells was mainly confined to the tumor tissues while levels in healthy tissues from tumor-bearing mice were only slightly increased compared to that in WT controls. This suggests that specific antigen stimulation is necessary for the boosted $CD8^+$ T-cell response and that T-cell specific PTPN2 depletion/inhibition would likely not affect non-tumor tissues. This unveils a therapeutic rationale for T-cell-specific PTPN2 inhibitors as an adjuvant therapy in CRC.

In line with the tumor-specific $CD8^+$ T-cell activation in the absence of PTPN2 in T-cells or DCs, we observed highly increased intratumoral infiltration of PTPN2-deficient $CD8^+$ T-cells. IFNγ-inducible chemokines, specifically CXCL9, CXCL10 and CXCL11 and their receptor CXCR3, have been described as important modulators of $CD8^+$ T-cell recruitment into tumor tissue (27-32). We have observed that PTPN2 deletion in T-cells and enhanced IFNγ signaling resulted in increased mRNA expression of many chemokines, but most significantly IFNγ-inducible CXCL9, CXCL11 and their receptor CXCR3, within the tumor tissue, highlighting enhanced potential to attract and accumulate cytotoxic T-cells within the tumor tissue. Hence, PTPN2 deficiency in T-cells not only enhances activity and cytotoxicity of tumor-infiltrating T-cells, but also facilitates their chemotaxis to the tumor.

PTPN2 deletion caused $CD8^+$ T-cells to be readily activated and enhanced their cytotoxicity and infiltration into tumor sites. In concurrence with the inverse correlation between PTPN2 and PD-1 in human CRC, we demonstrated that absence of PTPN2 in T-cells promoted the efficacy of anti-PD-1 therapy in mouse CRC, resulting in complete tumor clearance. In line with increased and sustained anti-PD-1 response, gene expression profiling revealed increased *Cxcr3* and *Cxcr5* mRNA expression - chemokine receptors crucial for efficient anti-PD-1 responses(30, 33) and memory formation (34, 35), respectively. Of importance for potential therapeutic strategies targeting PTPN2 in T cells, is the memory formation that mediated complete clearance of secondary tumors in mice lacking PTPN2 in T-cells, indicating that PTPN2-deletion/inhibition might not only serve as a potential treatment in primary CRC, but that such treatment might also significantly extend relapse-free survival.

Our data indicate that targeting PTPN2 represents a highly promising approach to enhance T cell tumor infiltration and tumor-specific cytotoxic activity and improve treatment response in tumors that are refractory to checkpoint inhibitors due to low immunogenicity and to prolong tumor-free survival via development of immune memory formation.

Methods

Human samples

Paraffin embedded human tissue slides used for PTPN2 and pSTAT1 were obtained from the Translational Research Center, Erlangen, Germany. RNA analysis has been performed by the Translational Research Center, Erlangen, Germany as described previously(36). A list of primers and probes can be found in Table S1. Cryopreserved non-tumor and colon tumor tissues for phosphatase activity assay and paraffin embedded primary colon tumor, liver and lung metastasis tissue slides for PTPN2, PD-1 and CTLA4 IHC stainings were obtained from the Pathology Department, University Hospital Zurich, Switzerland. The tissue microarray slides containing melanoma tissue for PTPN2 and PD1 staining were obtained from the Department of Dermatology, University Hospital Zurich, Switzerland.

Phosphatase activity assay

Samples for phosphatase activity measurements were homogenized using the genteMACS tissue homogenizer (Miltenyi) and proteins were per-cleared using Sepharose G beads (GE Healthcare) and then incubated overnight (o/n) at 4°C on a rocker with 10μg/mL rabbit anti-PTPN2 (Calbiochem; clone CF4-1D). Beads were added after o/n incubation and left on the rocker for 1h at 4°C. Precipitates were washed with PBS and phosphatase activity measured using EnzChek kit (Thermo Fisher Scientific). Fluorescence units (FU) measured every 10mins on a BioTek Synergy HT plate reader using Gene5 software.

Mice

C57BL/6N mice carrying *Cre* under the *Cd4* promoter were purchased from Taconic (Germany), CD11cCre-GFP line 4097 from The Jackson Laboratory (USA), *Ptpn2*$^{fl/fl}$ from EUCOMM (Germany), *APCmin* mice from The Jackson Laboratory (USA), *Rag2*$^{-/-}$ mice from Charles River (Germany) and OT1/J mice from The Jackson Laboratory (USA). All mice were kept in specific-pathogen-free conditions. *Ptpn2*$^{fl/fl}$ mice were bred with *Cd4*^{Cre} mice to obtain specific PTPN2 deletion in T-cells (17) and with *Cd11c*$^{Cre\text{-}GFP}$ mice to create specific deletion of PTPN2 in dendritic cells. Mice heterozygous for *Cd4*^{Cre} (*Ptpn2*$^{fl/fl}$*Cd4*$^{Cre+/-}$) or *Cd11c*^{Cre} (*Ptpn2*$^{fl/fl}$*Cd11*$^{Cre+/-}$) were bred with *Ptpn2*$^{fl/fl}$ (WT) mice to obtain *Cre*$^{+/-}$ and *Cre*$^{-/-}$ littermate controls (Ptpn2$^{fl/fl}$Cd4^{Cre-}/*Ptpn2*$^{fl/fl}$*CD4*$^{Cre+/-}$ and *Ptpn2*$^{fl/fl}$*Cd11cCre*$^{-}$/*Ptpn2*$^{fl/fl}$*Cd11c*$^{Cre+/-}$, respectively). Males and females between 8-12 weeks were used for all the experiments, except for AOM/DSS tumor induction, where only females were used. Littermate controls were used for all experiments. Mixed Ptpn2$^{fl/fl}$Cd4^{Cre-} and Ptpn2$^{fl/fl}$Cd11c^{Cre-} control mice (in the text and figures referred as Ptpn2fl/fl or WT controls) were used for AOM/DSS and cecum injection tumor models to minimize the required amount of animals. Whenever mixed control animals were used, both Ptpn2$^{fl/fl}$Cd4$^{Cre+/-}$ and Ptpn2$^{fl/fl}$Cd11$^{Cre+/-}$ groups were included in the same experiment and run in parallel. Experiments with mixed control groups are indicated in the figure legends.

Tumor models and treatments

Colitis-associated tumors were induced as described (19). DSS (MP Biomedicals, Carlsbad, CA) and AOM (Sigma Aldrich; 10mg/kg in saline). Controls receive water and were injected with saline. Mice were euthanized 10 days after the last DSS

treatment. After the third DSS cycle and at the end of the experiment, mice were anesthetized by i.p. injection of ketamine (90-120 mg kg^{-1} body weight; Vétoquinol, Bern, Switzerland) and Xylazine (8mg kg^{-1} body weight; Bayer, Lyssach, Switzerland) and colonoscopy performed to monitor tumor growth.

For injection models, MC38-GFP (donated by Prof. Lubor Borsig, Institute of Physiology, University of Zurich, Zurich) or B16-F10 tumor cells were suspended in culture medium, mixed 1:1 with matrigel and 300,000 cells, and injected into the cecum wall or subcutaneously into the mouse flank. Mice were euthanized 2-3 weeks after injection. In the subcutaneous model, tumor development was measured every 3 days using a digital caliper. Tumor volume was calculated using the ellipsoid formula: $4/3*3.14*Length/2*(Width/2)^2$ where the shorter dimension was used as width and depth. Mice were euthanized when the volume reached $1cm^3$ or the length reached 2cm.

CD8+ T-cells depletion was performed using anti-CD8 (Lyt 3.2) antibody (BioXCell; clone 53-5.8) or IgG isotype control (BioXCell; clone HRPN). Antibodies were injected i.p. in a concentration of 200mg/mouse on day -3 and 100mg/mouse on day 0 and once weekly afterwards. CD4+ T cells depletion was performed using anti-CD4 antibody (BioXCell; clone GK 1.5) or IgG isotype control (BioXCell; clone LTF-2). Antibodies were injected i.p. in a concentration of 200mg/mouse on day -3, day 0 and every 3 days afterwards. PD-1 blockade was performed in the subcutaneous tumor model and achieved by i.p. injection of 200mg/mouse anti-PD-1(CD279) antibody (BioXCell; clone 29F.1A12) or IgG isotype control (BioXCell; clone 2a3) on days 9, 12 and 15 after MC38 cells injection.

For adoptive transfer, 500,000 CD8+ T-cells from *Ptpn2fl/fl* and *Ptpn2*$^{fl/fl}$*Cd4*$^{Cre+/-}$ were transferred by i.p. injection into *Rag2*$^{-/-}$ mice on day 6 after the subcutaneous MC38 tumor injection.

Histology

Tumor and tumor-adjacent tissue from human patients, the most distal colon sections from the AOM/DSS experiment mice, and tumors from subcutaneous injection experiments were used for H&E, IHC and IF.

Tissues for immunofluorescence were deparaffinized and antigens retrieved using citrate buffer, pH 6.0 (Dako) at 98°C for 30min. Slides were kept in PBS with 10% goat serum, 10% BSA and 0.3% Triton X (Sigma-Aldrich) for 1h at RT to block the non-specific binding. Primary antibodies for IF was diluted in 1% BSA, 1% goat serum and 0.3% Triton X and incubated overnight at 4°C. A list of antibodies is given in Table S2. Slides were washed with 3% milk and PBS solution. Secondary goat anti-rabbit AF647 (Thermo Fisher Scientific) and goat anti-mouse AF594 (Thermo Fisher Scientific) were diluted in 1% BSA, 1% goat serum and 0.3% Triton X, slides incubated for 1h, washed with PBS and mounted. Fluorescent-labeled tissue sections were examined using the LEICA SP8 Upright and the LAS X (Leica) and LAS AF Lite software (Leica).

H&E was performed according to standard procedures. Tissues for IHC were deparaffinized and antigens retrieved using citrate buffer, pH 6.0 (Dako) at 98°C for 30min. Inhibition of endogenous peroxidases was performed by incubating tissue slides in 0.9% hydrogen peroxide for 15min at room temperature (RT). 2.5% horse serum for blocking non-specific binding was used for pSTAT1 and CD4 staining for 1h

at RT, for PTPN2 in human tissue, blocking solution was kept for 2h, and for CD3, CD8, PD-1, and CTLA4 staining 3% BSA was used for 1h. Primary antibodies were diluted in blocking solutions and slides incubated overnight at 4°C. A list of antibodies is given in Table S2. Secondary HRP-labeled antibody (Vector Laboratories, ImmPRESS) was applied for IHC samples for 1h at RT and staining visualized using the DAB ImmPACT Peroxidase Substrate brown kit (Vector Laboratories). IHC samples were counterstained with hematoxylin, dehydrated, and mounted. Tissue sections were examined using the Zeiss Axio Imager Z2 (Zeiss) and Zeiss 2.6 (blue edition) software (Zeiss).

Quantitative PCR

Healthy and tumor tissues (0.5cm) were homogenized using gentleMACS (Miltenyi Biotec, Bergisch Gladbach, Germany) and RNA isolated using the Maxwell RSC simplyRNA Tissu kit (Promega, Madison, WI, USA) according to the manufacturer's instructions. RNA concentration was measured using absorbance at 260 and 280 nm. Complementary DNA (cDNA) was synthesized using the high capacity cDNA reverse transcription kit (Thermo Fisher Scientific, Waltham, MA USA) according to the manufacturer's instructions. RT-PCR was performed using FAST qPCR Master Mix and pre-designed Taqman assays (Thermo Fisher Scientific, USA) on a QuantStudio 6 system using the QuantStudio software (Thermo Fisher Scientific, USA). Mouse GAPDH was used as endogenous control. Relative expression levels were calculated according to the $\Delta\Delta$CT method and samples were measured in triplicates.

Flow cytometry analysis

Spleen, mesenteric and skin draining lymph nodes, colon lamina propia lymphocytes, and tumor cells were used for flow cytometry analysis. Single cell suspensions from spleen, lymph nodes and LPL were prepared as described previously (37). Cecum and subcutaneous tumors were cut to approximately 0.5mm^3 pieces and digested in 6mL containing 0.5mg/mL collagenase type IV (Sigma Aldrich) and 0.05mg/mL DNAse I (Roche) solution for 10 minutes on a shaker (300 rpm) at 37°C. Cells were homogenized passing through 18G1.5 syringe and centrifuged for 10mins, 4°C, 1500 rpm. Single cell suspensions were stained and re-stimulated as described previously (38). Antibodies are listed in Table S3.

RNA isolation, sequencing, transcript quantification and differential expression analysis

Healthy, inflamed, and tumor tissue from AOM/DSS treated and water control *Ptpn2fl/fl* and *Ptpn2*$^{fl/fl}$*Cd4*$^{Cre+/-}$ mice were used for RNAseq analysis. RNA isolation and sequencing was performed by Microsynth, Balgach, Switzerland.

Transcripts were quantified with kallisto 0.44.0 (39) using the GRCm38 reference. Genes with a total transcript abundance quantification of < 10 were discarded from the downstream analysis. Differential expression analysis was performed in R (40) with DESeq2 (41) using the design formula ~genotype*treatment+tissue:genotype. Shrinkage of log2 fold changes was estimated using apeglm (42)**.** All sequencing data can be found in the ArrayExpress database. Accession number is E-MTAB-9629.

In vitro killing assay

For in vitro killing assay 50,000 MC38-GFP cells were stained with CellTrace Violet (Invitrogen), mixed with 50,000 MC-38-OVA-GFP cells stained with CellTrace Yellow (Invitrogen) and incubated for 24h at 37°C. Cells were then kept alone or co-cultured with enriched $CD8^+$ T-cells from spleen of either *Ptpn2*$^{fl/fl}$*Cd4*$^{Cre-}$*OT I* or *Ptpn2*$^{fl/fl}$*Cd4*$^{Cre+/-}$*OT I* mice for 24h in a 37°C incubator. $CD8^+$ T-cells were enriched using EasySep $CD8^+$ T-cells enrichment kit (Stemcell Technologies). Apoptosis was then detected using Annexin V kit – DY-634 antibody (Abcam) and Zombie NIR fixable viability kit (Biolegend).

Statistics

For 2 group comparisons, non-parametric two-tailed Mann Whitney test was used, while for 3 or more groups, one-way ANOVA followed by Tukey's multiple comparisons test was used. All experiments, which were performed in parallel were analyzed together and later separated into different graphs to demonstrate results in different figures. For RNA sequencing analysis false sign rate was used to determine significances. All p-values are indicated in the figures and $p<0.05$ was considered significant.

Study approval

All tissues were collected in accordance to local ethical regulations and patients have given written informed consent prior to sample collection. The study was approved by the Cantonal Ethics Committee of the Canton Zürich, Switzerland (approval no. 2018-

02193 and KEK-ZH-647) and the local ethics committee of the Friedrich-Alexander-University (FAU) of Erlangen-Nürnberg.

All animal experiments were performed according to Swiss animal welfare legislation and approved by the local veterinary office (Veterinäramt des Kantons Zürich) (License numbers 239/2016 and 179/2019).

Author Contributions: E.K.: Data acquisition, analysis, interpretation, drafting the manuscript; L.H., A.M.A., P.B., Ma.Sc., R.M., J.C.A., K.A., S.La., E.N.: data acquisition and analysis; V.S.S., M.St., A.R., M.T., A.W., S.Le., M.L.,: acquisition of patient material, data interpretation; G.E.L.: data analysis and interpretation; O.B., G.R.: data interpretation; Mi.Sc.: conceived study, study design, supervision, data interpretation, funding; M.R.S.: study design, supervision, data interpretation.

Acknowledgements: Flow cytometry was performed with equipment of the flow cytometry facility, University of Zurich. We thank Miro E. Raeber (Department of Immunology, University Hospital Zurich, Zurich) for his technical support with CD4+ T cells depletion experiment.

Funding: Stiftung Experimentelle Biomedizin to M.Sc., SNSF 314730_166381 and SNSF 320030_184753 to M.Sc., Novartis Foundation for Biomedical Research to M.Sc., DFG-FOR2438 to E.N./M.St. and DFG-TRR241 to M.St.

References

1. Ciardiello D, Vitiello PP, Cardone C, Martini G, Troiani T, Martinelli E, et al. Immunotherapy of colorectal cancer: Challenges for therapeutic efficacy. *Cancer Treat Rev.* 2019;76:22-32.
2. Ganesh K, Stadler ZK, Cercek A, Mendelsohn RB, Shia J, Segal NH, et al. Immunotherapy in colorectal cancer: rationale, challenges and potential. *Nat Rev Gastroenterol Hepatol.* 2019;16(6):361-75.
3. Bray F, Ferlay J, Soerjomataram I, Siegel RL, Torre LA, and Jemal A. Global cancer statistics 2018: GLOBOCAN estimates of incidence and mortality worldwide for 36 cancers in 185 countries. *CA Cancer J Clin.* 2018;68(6):394-424.
4. Montalban-Arques A, and Scharl M. Intestinal microbiota and colorectal carcinoma: Implications for pathogenesis, diagnosis, and therapy. *EBioMedicine.* 2019.
5. Rawla P, Barsouk A, Hadjinicolaou AV, and Barsouk A. Immunotherapies and Targeted Therapies in the Treatment of Metastatic Colorectal Cancer. *Med Sci (Basel).* 2019;7(8).
6. Umezawa S, Higurashi T, Komiya Y, Arimoto J, Horita N, Kaneko T, et al. Chemoprevention of colorectal cancer: Past, present, and future. *Cancer Sci.* 2019;110(10):3018-26.
7. Passarelli A, Mannavola F, Stucci LS, Tucci M, and Silvestris F. Immune system and melanoma biology: a balance between immunosurveillance and immune escape. *Oncotarget.* 2017;8(62):106132-42.

8. Givechian KB, Garner C, Benz S, Song B, Rabizadeh S, and Soon-Shiong P. An immunogenic NSCLC microenvironment is associated with favorable survival in lung adenocarcinoma. *Oncotarget.* 2019;j10(19):1840-9.
9. Kalyan A, Kircher S, Shah H, Mulcahy M, and Benson A. Updates on immunotherapy for colorectal cancer. *J Gastrointest Oncol.* 2018;9(1):160-9.
10. Arora SP, and Mahalingam D. Immunotherapy in colorectal cancer: for the select few or all? *J Gastrointest Oncol.* 2018;9(1):170-9.
11. Manguso RT, Pope HW, Zimmer MD, Brown FD, Yates KB, Miller BC, et al. In vivo CRISPR screening identifies Ptpn2 as a cancer immunotherapy target. *Nature.* 2017;547(7664):413-8.
12. LaFleur MW, Nguyen TH, Coxe MA, Miller BC, Yates KB, Gillis JE, et al. PTPN2 regulates the generation of exhausted CD8(+) T cell subpopulations and restrains tumor immunity. *Nat Immunol.* 2019;20(10):1335-47.
13. Wiede F, Lu KH, Du X, Liang S, Hochheiser K, Dodd GT, et al. PTPN2 phosphatase deletion in T cells promotes anti-tumour immunity and CAR T-cell efficacy in solid tumours. *Embo j.* 2019:e103637.
14. Wiede F, Shields BJ, Chew SH, Kyparissoudis K, van Vliet C, Galic S, et al. T cell protein tyrosine phosphatase attenuates T cell signaling to maintain tolerance in mice. *J Clin Invest.* 2011;121(12):4758-74.
15. Scharl M, Hruz P, and McCole DF. Protein tyrosine phosphatase non-receptor Type 2 regulates IFN-gamma-induced cytokine signaling in THP-1 monocytes. *Inflamm Bowel Dis.* 2010;16(12):2055-64.
16. Scharl M, McCole DF, Weber A, Vavricka SR, Frei P, Kellermeier S, et al. Protein tyrosine phosphatase N2 regulates TNFalpha-induced signalling and cytokine secretion in human intestinal epithelial cells. *Gut.* 2011;60(2):189-97.

17. Spalinger MR, Kasper S, Chassard C, Raselli T, Frey-Wagner I, Gottier C, et al. PTPN2 controls differentiation of CD4(+) T cells and limits intestinal inflammation and intestinal dysbiosis. *Mucosal Immunol.* 2015;8(4):918-29.
18. Heinonen KM, Nestel FP, Newell EW, Charette G, Seemayer TA, Tremblay ML, et al. T-cell protein tyrosine phosphatase deletion results in progressive systemic inflammatory disease. *Blood.* 2004;103(9):3457-64.
19. Spalinger MR, Manzini R, Hering L, Riggs JB, Gottier C, Lang S, et al. PTPN2 Regulates Inflammasome Activation and Controls Onset of Intestinal Inflammation and Colon Cancer. *Cell Rep.* 2018;22(7):1835-48.
20. Alcantara M, Simonin M, Lhermitte L, Touzart A, Dourthe ME, Latiri M, et al. Clinical and biological features of PTPN2-deleted adult and pediatric T-cell acute lymphoblastic leukemia. *Blood Adv.* 2019;3(13):1981-8.
21. Wiede F, Dudakov JA, Lu KH, Dodd GT, Butt T, Godfrey DI, et al. PTPN2 regulates T cell lineage commitment and alphabeta versus gammadelta specification. *J Exp Med.* 2017;214(9):2733-58.
22. Sharma S, and Zhu J. Immunologic applications of conditional gene modification technology in the mouse. *Curr Protoc Immunol.* 2014;105:10.34.1-10.34.13.
23. Lee PP, Fitzpatrick DR, Beard C, Jessup HK, Lehar S, Makar KW, et al. A critical role for Dnmt1 and DNA methylation in T cell development, function, and survival. *Immunity.* 2001;15(5):763-74.
24. Hering L, Katkeviciute E, Schwarzfischer M, Busenhart P, Gottier C, Mrdjen D, et al. Protein Tyrosine Phosphatase Non-Receptor Type 2 Function in Dendritic Cells Is Crucial to Maintain Tissue Tolerance. *Front Immunol.* 2020;11(1856).

25. de Vries NL, Swets M, Vahrmeijer AL, Hokland M, and Kuppen PJ. The Immunogenicity of Colorectal Cancer in Relation to Tumor Development and Treatment. *Int J Mol Sci.* 2016;17(7).

26. Van der Jeught K, Xu HC, Li YJ, Lu XB, and Ji G. Drug resistance and new therapies in colorectal cancer. *World J Gastroenterol.* 2018;24(34):3834-48.

27. Kistner L, Doll D, Holtorf A, Nitsche U, and Janssen KP. Interferon-inducible CXC-chemokines are crucial immune modulators and survival predictors in colorectal cancer. *Oncotarget.* 2017;8(52):89998-90012.

28. Metzemaekers M, Vanheule V, Janssens R, Struyf S, and Proost P. Overview of the Mechanisms that May Contribute to the Non-Redundant Activities of Interferon-Inducible CXC Chemokine Receptor 3 Ligands. *Front Immunol.* 2017;8:1970.

29. Tokunaga R, Zhang W, Naseem M, Puccini A, Berger MD, Soni S, et al. CXCL9, CXCL10, CXCL11/CXCR3 axis for immune activation - A target for novel cancer therapy. *Cancer Treat Rev.* 2018;63:40-7.

30. Chow MT, Ozga AJ, Servis RL, Frederick DT, Lo JA, Fisher DE, et al. Intratumoral Activity of the CXCR3 Chemokine System Is Required for the Efficacy of Anti-PD-1 Therapy. *Immunity.* 2019;50(6):1498-512.e5.

31. Peng D, Kryczek I, Nagarsheth N, Zhao L, Wei S, Wang W, et al. Epigenetic silencing of TH1-type chemokines shapes tumour immunity and immunotherapy. *Nature.* 2015;527(7577):249-53.

32. Zingg D, Arenas-Ramirez N, Sahin D, Rosalia RA, Antunes AT, Haeusel J, et al. The Histone Methyltransferase Ezh2 Controls Mechanisms of Adaptive Resistance to Tumor Immunotherapy. *Cell Rep.* 2017;20(4):854-67.

33. Han X, Wang Y, Sun J, Tan T, Cai X, Lin P, et al. Role of CXCR3 signaling in response to anti-PD-1 therapy. *EBioMedicine.* 2019.

34. Im SJ, Hashimoto M, Gerner MY, Lee J, Kissick HT, Burger MC, et al. Defining CD8+ T cells that provide the proliferative burst after PD-1 therapy. *Nature.* 2016;537(7620):417-21.

35. Perdomo-Celis F, Taborda NA, and Rugeles MT. Follicular CD8(+) T Cells: Origin, Function and Importance during HIV Infection. *Front Immunol.* 2017;8:1241-.

36. Naschberger E, Liebl A, Schellerer VS, Schutz M, Britzen-Laurent N, Kolbel P, et al. Matricellular protein SPARCL1 regulates tumor microenvironment-dependent endothelial cell heterogeneity in colorectal carcinoma. *J Clin Invest.* 2016;126(11):4187-204.

37. Spalinger MR, Kasper S, Gottier C, Lang S, Atrott K, Vavricka SR, et al. NLRP3 tyrosine phosphorylation is controlled by protein tyrosine phosphatase PTPN22. *J Clin Invest.* 2016;126(5):1783-800.

38. Spalinger MR, Schwarzfischer M, Hering L, Shawki A, Sayoc A, Santos A, et al. Loss of PTPN22 abrogates the beneficial effect of cohousing-mediated fecal microbiota transfer in murine colitis. *Mucosal Immunol.* 2019.

39. Bray NL, Pimentel H, Melsted P, and Pachter L. Near-optimal probabilistic RNA-seq quantification. *Nat Biotechnol.* 2016;34(5):525-7.

40. Team RC. R: A language and environment for statistical computing. *R Found for Stat Comp.* 2019.

41. Love MI, Huber W, and Anders S. Moderated estimation of fold change and dispersion for RNA-seq data with DESeq2. *Genome Biol.* 2014;15(12):550.

42. Zhu A, Ibrahim JG, and Love MI. Heavy-tailed prior distributions for sequence count data: removing the noise and preserving large differences. *Bioinform* 2019;35(12):2084-92.

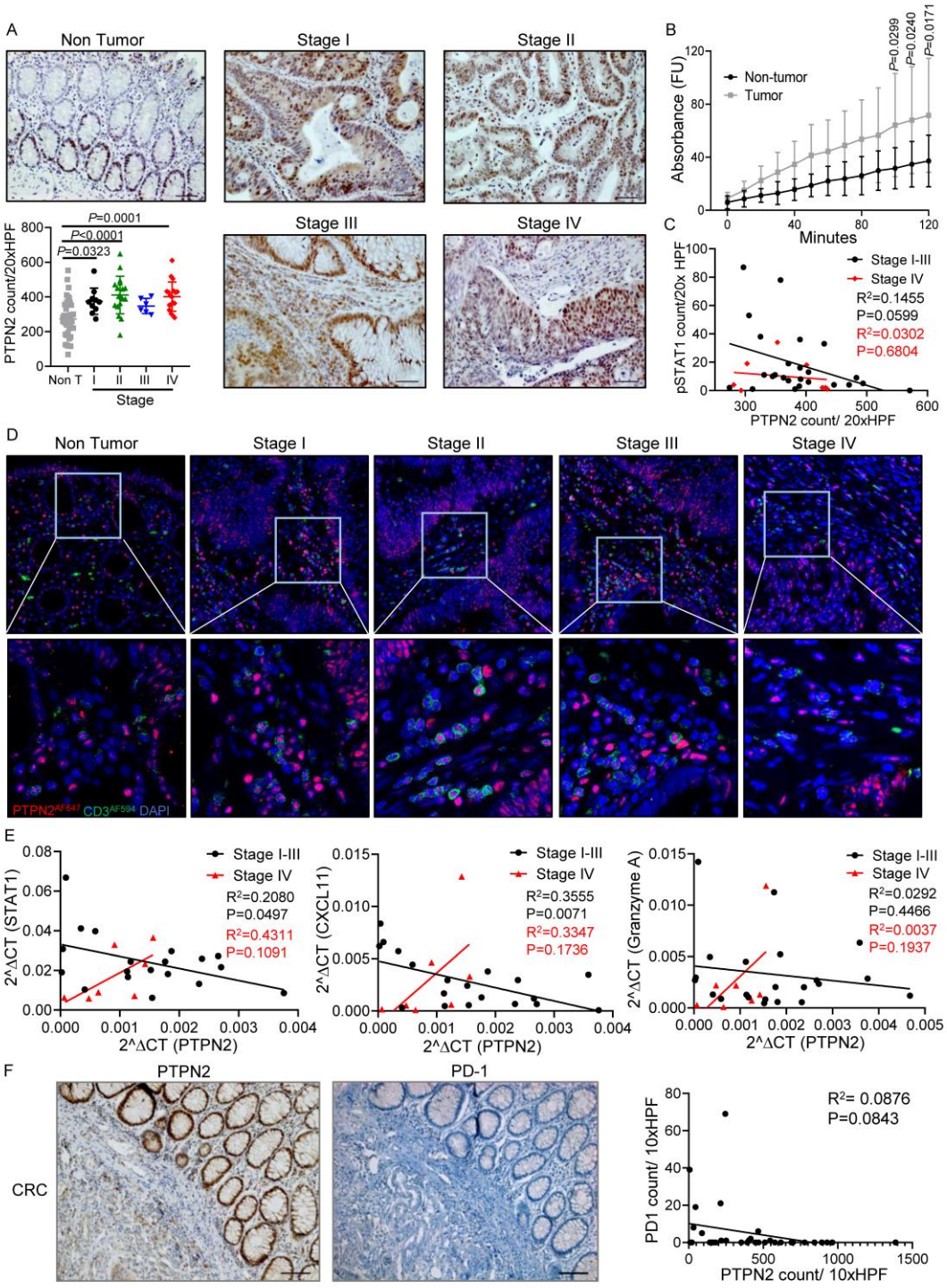

Figure 1. Enhanced PTPN2 expression in human colorectal carcinoma. (**A**) Representative images and quantification of PTPN2 immunohistochemistry (IHC) staining in non-tumor (Non T) and stage I-IV tumor tissue. Scale bar represents 50μm. One-way ANOVA, Tukey's multiple comparisons test. (**B**) PTPN2 phosphatase activity in non-tumor and tumor tissue (n=10 samples per condition). Two-tailed Mann Whitney test. (**C**) Correlation between PTPN2 and pSTAT1 protein quantification and (**D**) immunofluorescence co-staining of CD3 (AF594 green), PTPN2 (AF647 red) and DAPI. 40x magnification and zoom factor set to 3.0. (**E**) Correlations between mRNA expression of *PTPN2* gene and *STAT1, CXCL11* and *GRZA* genes. Linear regression; p values and R^2 indicated. (**F**) Representative images of IHC and correlations of PTPN2 and checkpoint molecule PD-1 in primary CRC Scale bar represents 100μm. Linear regression; all p values and R^2 are indicated in the figure.

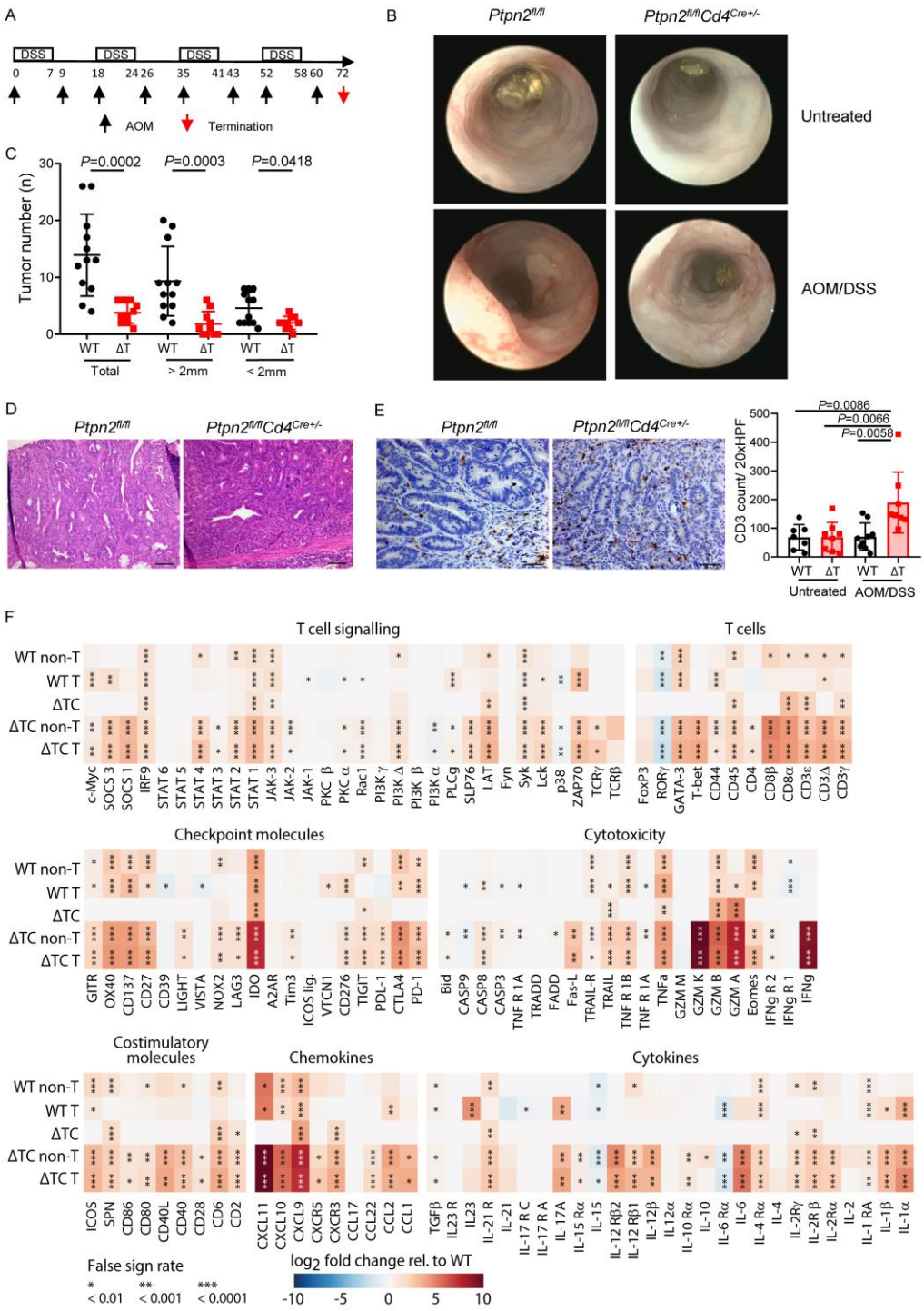

Figure 2. PTPN2 deletion in T-cells leads to reduced tumor load in colitis-associated tumors. Tumors were induced in *Ptpn2*$^{fl/fl}$*Cd4*$^{Cre+/-}$ mice (ΔT) (n=10) and their littermate controls *Ptpn2*$^{fl/fl}$ (WT) (n=12) using the AOM/DSS model (2 independent experiments). Mixed WT controls (*Ptpn2*$^{fl/fl}$*Cd4*$^{Cre-}$ and *Ptpn2*$^{fl/fl}$*Cd11c*$^{Cre-}$) were used in this experiment. (**A**) Schematic overview of the experimental procedure. (**B**) Representative colonoscopy pictures from untreated and AOM/DSS treated mice. Two-tailed Mann Whitney test. (**C**) Quantification of the tumor number in total, and stratified by tumor size. (**D**) H&E staining of tumor tissue from *Ptpn2*$^{fl/fl}$*Cd4*$^{Cre+/-}$ and *Ptpn2*$^{fl/fl}$ mice. Scale bar represents 100μm. (**E**) Representative images and quantification of CD3 staining in ΔT and WT tumor tissue. Scale bar: 50μm. One-way ANOVA, Tukey's multiple comparisons test; RNA-Seq was performed on untreated, inflamed non-tumor and inflamed tumor tissue in *Ptpn2*$^{fl/fl}$ and *Ptpn2*$^{fl/fl}$*Cd4*$^{Cre+/-}$ mice, n=4, each. (**F**) Heat map of mRNA expression levels of T-cell-related genes from WT inflamed non-tumor, WT inflamed tumor tissue, ΔT untreated tissue, ΔT inflamed non-tumor and ΔT inflamed tumor tissue normalized to the expression in colon tissue from water-treated WT mice. False sign rate *<0.01, **<0.001, ***<0.0001. Lines and error bars in the dot plots represent means with standard deviation.

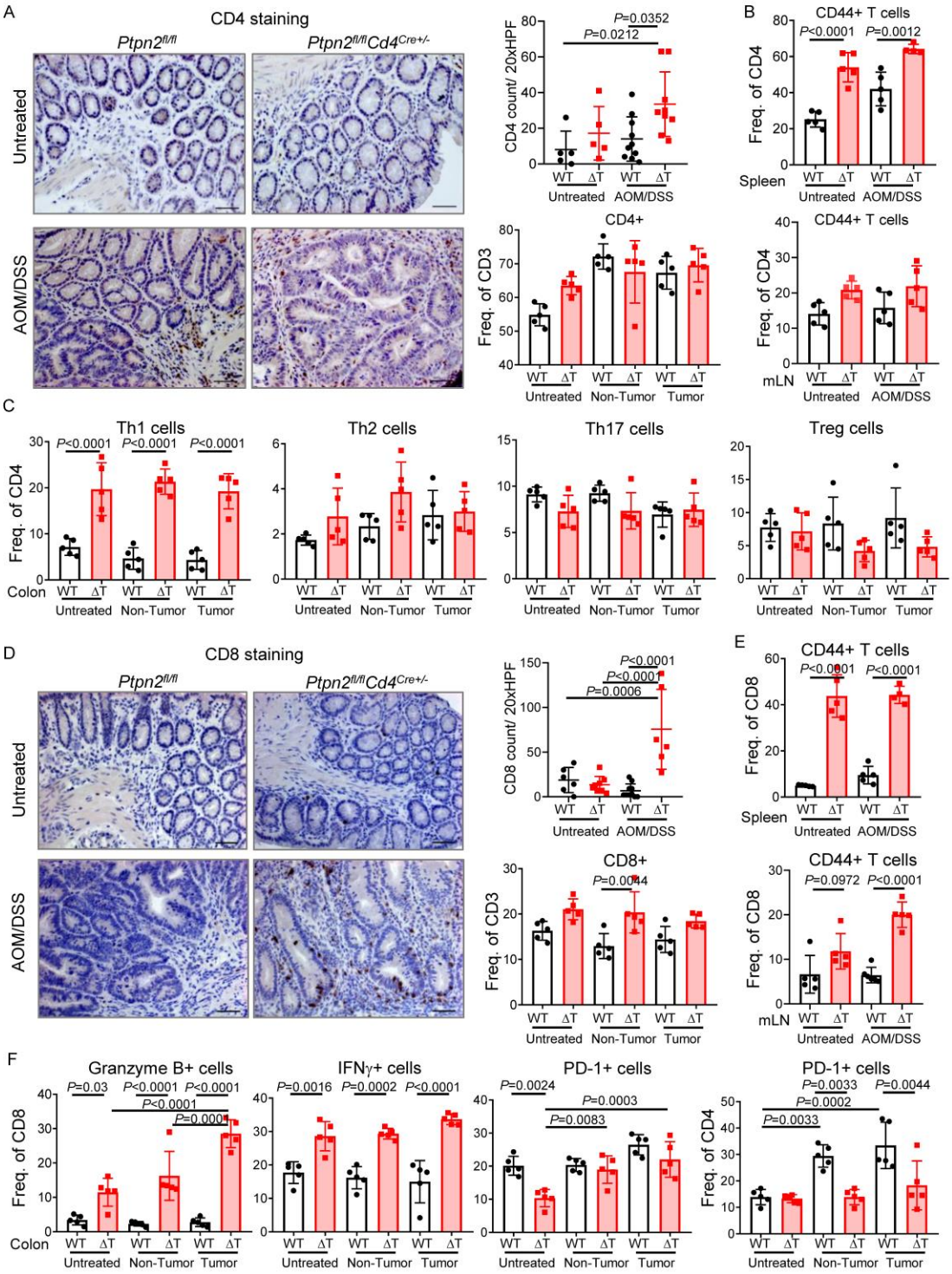

Figure 3. PTPN2 deletion in T-cells promotes T-cell activation in tumor tissue. Tumors were induced as described in Figure 2. (**A**) Representative images and quantification of CD4 IHC staining and flow cytometry on WT and ΔT untreated and tumor tissue. Scale bar represents 50μm. One-way ANOVA, Tukey's multiple comparisons test; Flow cytometry analysis of untreated colon (water group; n=5mice), inflamed non-tumor and inflamed tumor tissue (n=5mice). (**B** and **C**) Frequencies of $CD4^+$ T-cells, effector/memory $CD4^+CD44^+$ T-cells (spleen and mesenteric lymph nodes (mLN)), and Th1 ($CD4^+IFNg^+$), Th2 ($CD4^+IL\text{-}4^+$), Th17 ($CD4^+IL\text{-}17^+$), and Tregs ($CD4^+FoxP3^+$) (colon). One-way ANOVA, Tukey's multiple comparisons test; (**D**) Localization and quantification of $CD8^+$ cells in *Ptpn2*$^{fl/fl}$*Cd4*$^{Cre+/-}$ and *Ptpn2*$^{fl/fl}$ untreated and tumor tissue. Scale bar represents 50μm. One-way ANOVA, Tukey's multiple comparisons test; (**E**) Frequencies of effector/memory $CD8^+CD44^+$ T-cells (spleen and mLN). One-way ANOVA, Tukey's multiple comparisons test; (**F**) Frequencies of CD8+granzyme B+, CD8+IFNγ+ and checkpoint molecule PD-1 on $CD4^+$ and $CD8^+$ T-cells. One-way ANOVA, Tukey's multiple comparisons test. Lines and error bars in the dot plots represent means with standard deviation.

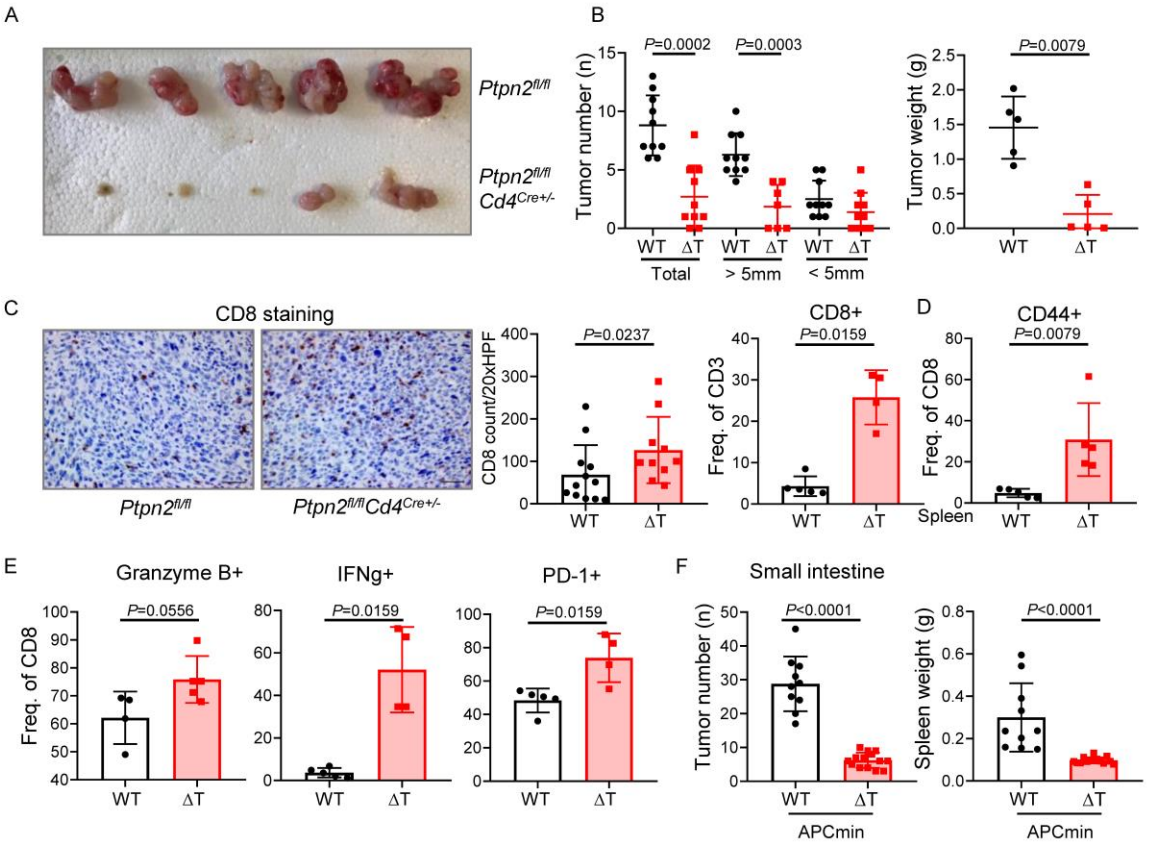

Figure 4. Reduced tumor burden in orthotopic tumor injection and APCmin tumor models upon PTPN2 deletion in T-cells. 300'000 MC38 tumor cells were injected into the cecum wall to *Ptpn2*$^{fl/fl}$ (WT) and *Ptpn2*$^{fl/fl}$*Cd4*$^{Cre+/-}$(ΔT) mice. Mixed WT controls (*Ptpn2*$^{fl/fl}$*Cd4*$^{Cre-}$ and *Ptpn2*$^{fl/fl}$*Cd11c*$^{Cre-}$) were used in this experiment, thus WT quantification in C is the same as WT quantification in Fig. 7F. (**A**) Representative pictures of cecum tumors from *Ptpn2*$^{fl/fl}$ and *Ptpn2*$^{fl/fl}$*Cd4*$^{Cre+/-}$ mice (n=5mice). (**B**) Numbers of tumors in total, stratified according to size (n=10 mice; 2 independent experiments), and tumor weight (n=5 mice). Two-tailed Mann Whitney test. (**C**) Representative images and quantification of IHC staining and flow cytometry of CD8 staining in *Ptpn2*$^{fl/fl}$ and *Ptpn2*$^{fl/fl}$*Cd4*$^{Cre+/-}$ tumor tissue. Scale bar represents 50μm. Two-tailed Mann Whitney test. Frequencies of effector/memory CD8^{+}CD44^{+} T-cells in spleen (**D**) and granzyme B, IFNg and PD-1 (**E**). Two-tailed Mann Whitney test. (**F**) Number of tumors in the small intestine and spleen weight of *Ptpn2*$^{fl/fl}$*APCmin* and *Ptpn2*$^{fl/fl}$*Cd4*$^{Cre+/-}$*APCmin* mice. Two-tailed Mann Whitney test.

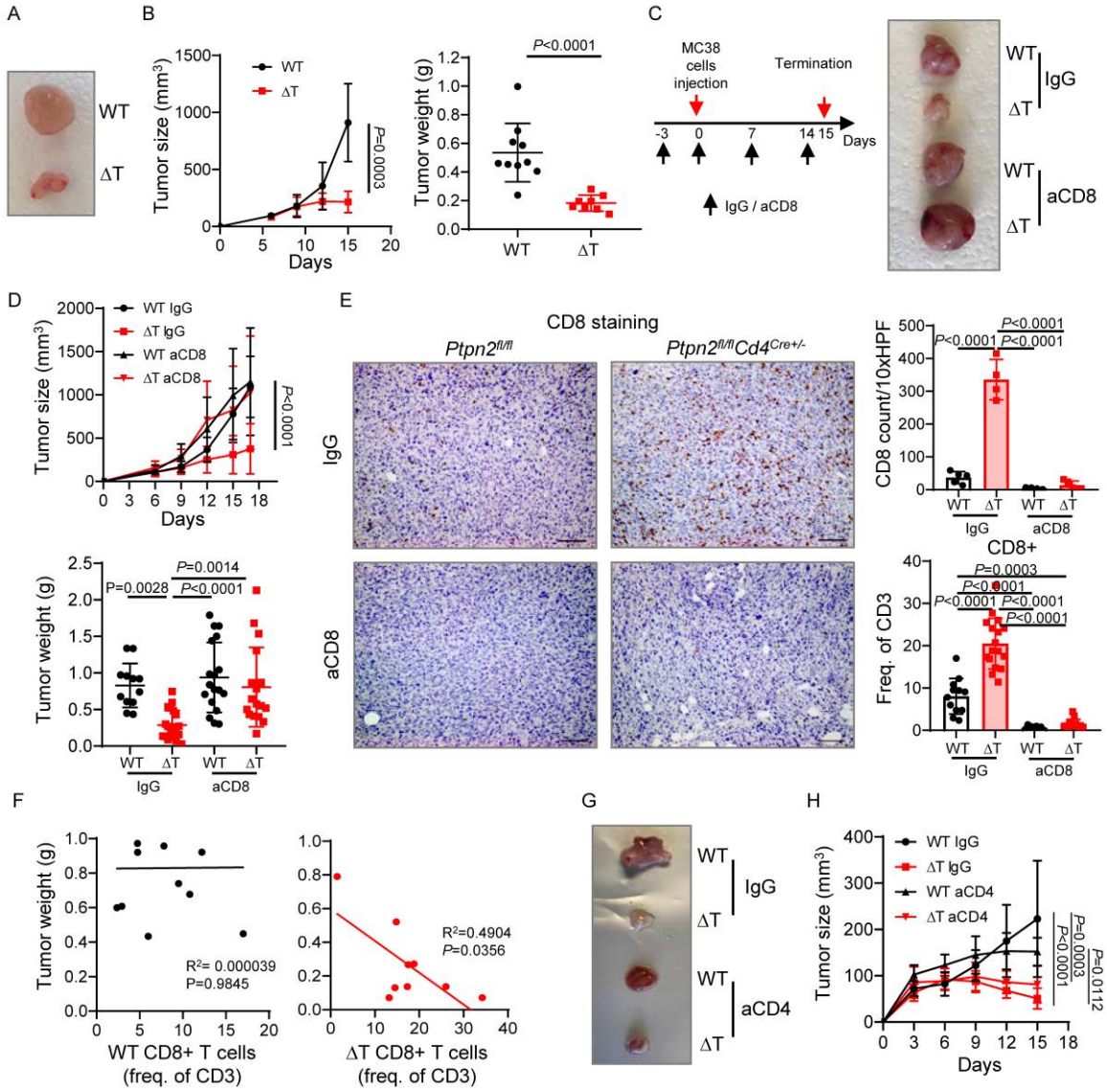

Figure 5. CD8$^+$ T-cells are the key drivers of tumor reduction. 300'000 MC38 tumor cells were injected subcutaneously to *Ptpn2*$^{fl/fl}$ and *Ptpn2*$^{fl/fl}$*Cd4*$^{Cre+/-}$ mice. (**A**) Representative images of s.c. MC38 in *Ptpn2*$^{fl/fl}$ (WT) and *Ptpn2*$^{fl/fl}$*Cd4*$^{Cre+/-}$ (ΔT) mice. (**B**) MC38 (WT n=5 mice/ 10 tumors, ΔT n=4 mice/ 8 tumors) tumor development over time and tumor weight at the last day of the experiment. Two-tailed Mann Whitney test. (**C**) Scheme of CD8$^+$ T-cell depletion and image of representative tumors from IgG isotype control and anti-CD8 treated WT and ΔT mice. (**D**) Tumor development and tumor weight (WT IgG n=6 mice/ 12 tumors, ΔT IgG, WT anti-CD8 and ΔT anti-CD8 n=10 mice/ 20 tumors; 2 independent experiments). One-way ANOVA, Tukey's multiple comparisons test. (**E**) Representative images and quantification of immunohistochemistry and flow cytometry CD8 staining in *Ptpn2*$^{fl/fl}$ and *Ptpn2*$^{fl/fl}$*Cd4*$^{Cre+/-}$ mouse tumor tissue from IgG control and anti-CD8 treated groups. Scale bar represents 50μm. One-way ANOVA, Tukey's multiple comparisons test. (**F**) Inverse correlation of tumor weight and frequencies of CD8+T-cells in tumor tissue from WT and ΔT mice. Linear regression; p values and R^2 indicated. (**G**) Representative images of MC38 tumors from IgG isotype control and anti-CD4 treated WT and ΔT mice. (**H**) Tumor development (n=5mice/ 10 tumors per group). One-way ANOVA, Tukey's multiple comparisons test. Lines and error bars in the dot plots represent means with standard deviation.

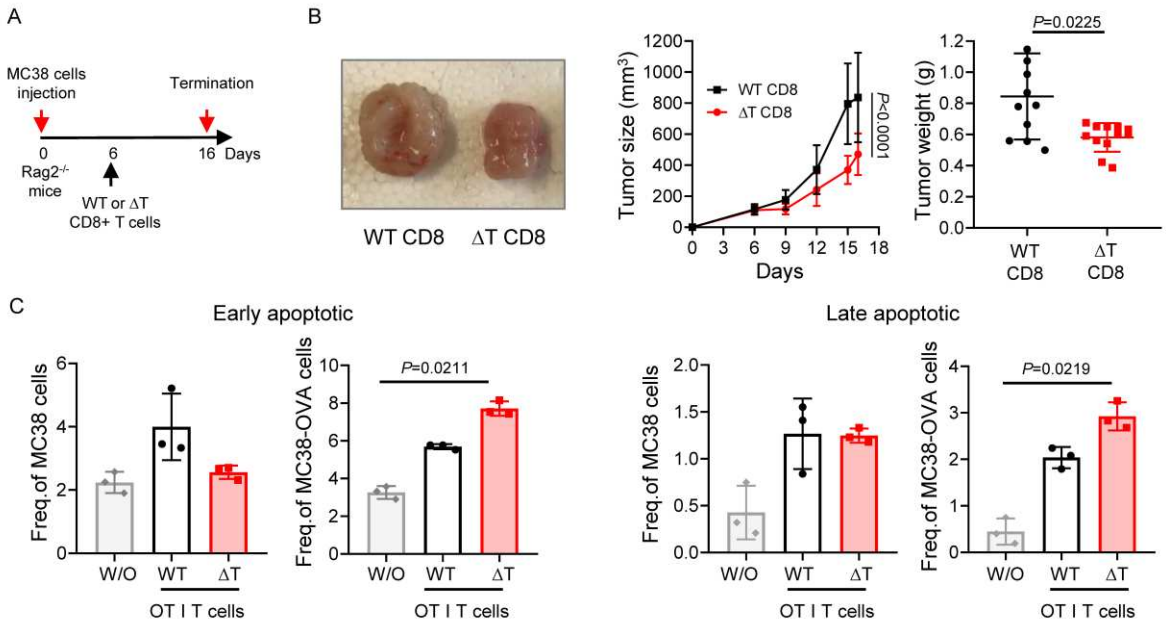

Figure 6. Tumor reduction after therapeutic PTPN2-deficient CD8+ T cells transfer**.** (**A**) Scheme of WT or ΔT CD8^{+} T-cell transfer into *Rag2*$^{-/-}$ mice. (**B***)* Representative image, development curve and weight of MC38 tumors from mice without T-cell transfer (n=6 mice/ 12 tumors) or with either WT CD8^{+} T-cells (n=5 mice/ 10 tumors) or ΔT CD8^{+} T-cells transfer (n=6 mice/ 12 tumors). Two-tailed Mann Whitney test. (**C**) in vitro killing assay of MC38 and MC38-OVA cells by WT and ΔT OT-I T cells. Graphs represent early (Annexin V^{+}ZombieNIR^{-}) and late apoptotic (Annexin V^{+}ZombieNIR^{+}) cells. One-way ANOVA, Tukey's multiple comparisons test. Lines and error bars in the dot plots represent means with standard deviation.

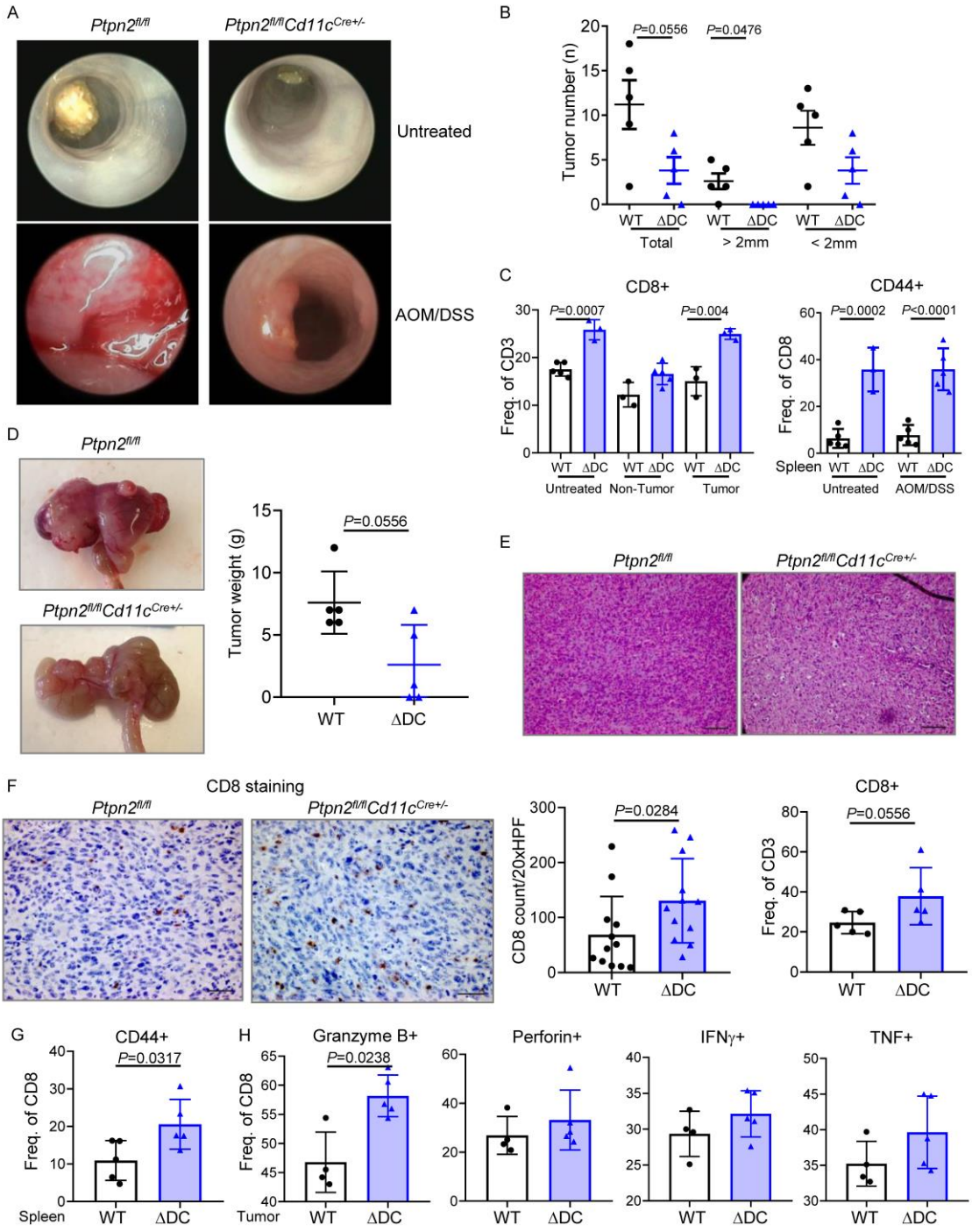

Figure 7. PTPN2 deletion in dendritic cells (DCs) leads to reduced tumor load in the AOM/DSS and in the othotopic injection model. Tumor development was induced in *Ptpn2*$^{fl/fl}$ (WT; n=5 mice) and their *Ptpn2*$^{fl/fl}$*Cd11c*$^{Cre+/-}$ littermate (ΔDC; n=5 mice) using the AOM/DSS model and the cecum injection model. Mixed WT controls (*Ptpn2*$^{fl/fl}$*Cd4*$^{Cre-}$ and *Ptpn2*$^{fl/fl}$*Cd11c*$^{Cre-}$) were used in these experiments, thus WT quantification in F is the same as WT quantification in Fig. 4C. (**A**) Representative colonoscopy pictures. (**B**) Quantification of the tumor number in total, and according to tumor size. Two-tailed Mann Whitney test. Flow cytometry analysis was performed on healthy colon, inflamed non-tumor and inflamed tumor tissue. (**C**) Frequencies of CD8+ T-cells (colon) and effector/memory CD8+CD44+ T-cells (spleen). Two-tailed Mann Whitney test. (**D**) Pictures of the cecum and tumor weight from WT and ΔDC mice. (**E**) H&E staining of the tumor tissue from *Ptpn2*$^{fl/fl}$ and *Ptpn2*$^{fl/fl}$*Cd11c*$^{Cre+/-}$ mice. Scale bar represents 100μm. (**F**) Representative images and quantification of IHC and flow cytometry frequency of CD8 staining in WT and ΔDC mouse tumor tissue. Scale bar represents 50μm. Two-tailed Mann Whitney test. (**G** and **H**) Frequencies of effector/memory CD8+CD44+ T-cells (spleen), and the cytotoxicity markers granzyme B, perforin, IFNγ, and TNF (tumor). Two-tailed Mann Whitney test Lines and error bars in the dot plots represent means with standard deviation.

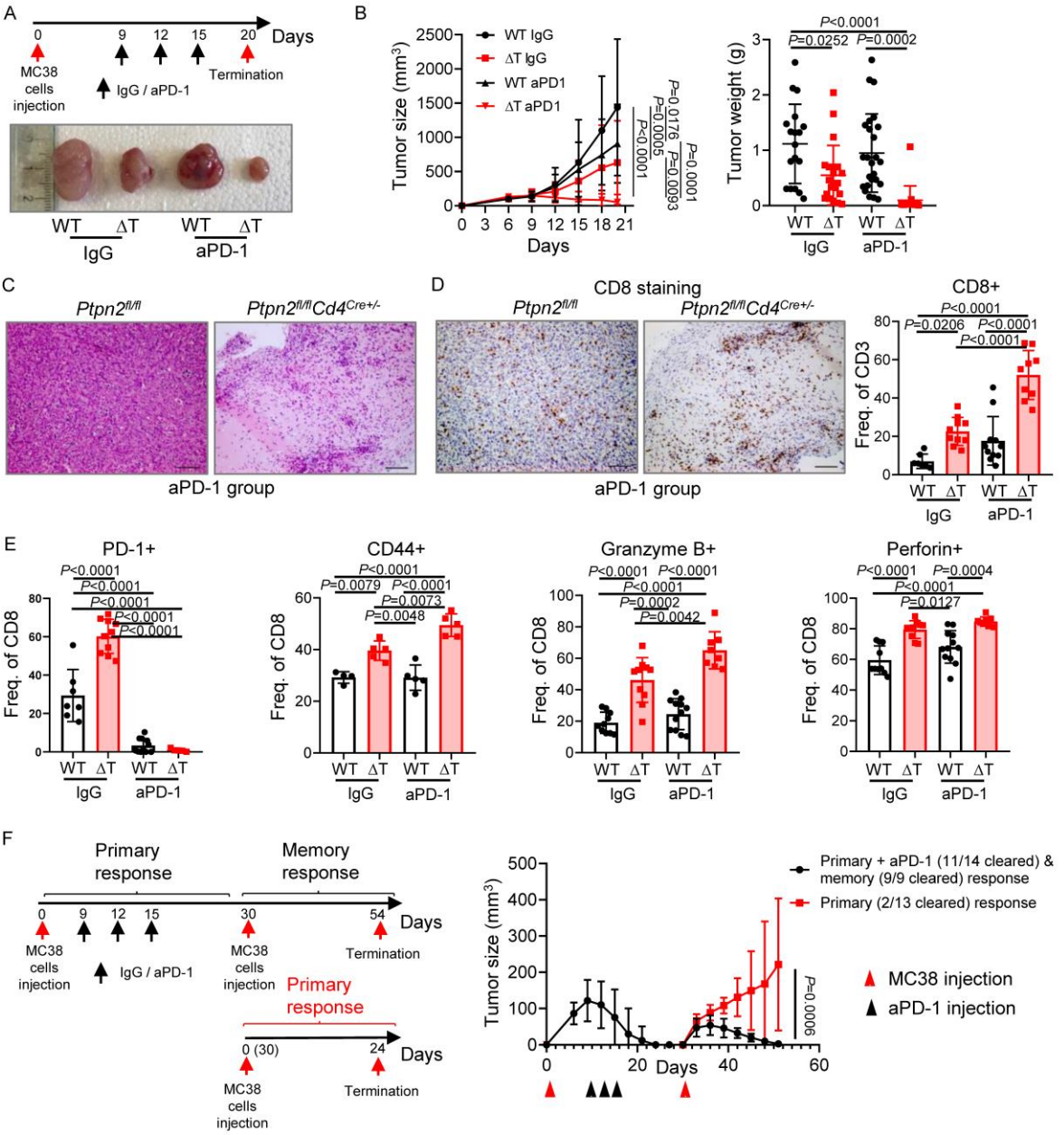

Figure 8. PTPN2 deficiency and anti-PD-1 therapy leads to enhanced synergetic anti-tumor response. (**A**) Schematic overview of the treatment and representative pictures of tumors in *Ptpn2*$^{fl/fl}$(WT) and *Ptpn2*$^{fl/fl}$*Cd4*$^{Cre+/-}$ (ΔT) mice treated with IgG control or anti-PD-1 antibody. (**B**) Tumor development and weight (n=10 mice/ 20 tumors; 2 independent experiments). One-way ANOVA, Tukey's multiple comparisons test. (**C**) H&E staining of the tumor tissue from *Ptpn2*$^{fl/fl}$ and *Ptpn2*$^{fl/fl}$*Cd4*$^{Cre+/-}$ mice. Scale bar represents 100μm. (**D**) Representative images of immunohistochemistry staining and flow cytometry frequency of CD8 staining in *Ptpn2*$^{fl/fl}$ and *Ptpn2*$^{fl/fl}$*Cd4*$^{Cre+/-}$ mice tumor tissue. Scale bar represents 100μm. One-way ANOVA, Tukey's multiple comparisons test. (**E**) Frequencies of PD-1, CD44, granzyme B and perforin on CD8^{+} T-cells from IgG control and anti-PD-1 groups. One-way ANOVA, Tukey's multiple comparisons test. (**F**) Outline of the primary and memory response experiment and tumor development curve in *Ptpn2*$^{fl/fl}$*Cd4*$^{Cre+/-}$ mice (first primary n=7 mice, 14 tumors; memory n=7mice, 9 tumors; second primary n=13 mice, 13 tumors; 2 independent experiments). One-way ANOVA, Tukey's multiple comparisons test. Lines and error bars in the dot plots represent means with standard deviation.